Focusing of phase change microparticles for local heat transfer enhancement in laminar flows

Citation: Lenert, Andrej; Nam, Youngsuk; Yilbas, Bekir S. and Wang, Evelyn N. "Focusing of phase change microparticles for local heat transfer enhancement in laminar flows." International Journal of Heat and Mass Transfer 56, no. 1-2 (January 2013): 380-389. © 2012 Elsevier Ltd

As Published: http://dx.doi.org/10.1016/j.ijheatmasstransfer.2012.09.014

Publisher: Elsevier

Persistent URL: http://hdl.handle.net/1721.1/108293

Version: Author's final manuscript: final author's manuscript post peer review, without publisher's formatting or copy editing

DOI: 10.1016/j.ijheatmasstransfer.2012.09.014

Source: Lenert, Andrej, Youngsuk Nam, Bekir S. Yilbas, and Evelyn N. Wang. "Focusing of Phase Change Microparticles for Local Heat Transfer Enhancement in Laminar Flows." International Journal of Heat and Mass Transfer 56, no. 1–2, p. 380–389, 2013.

Focusing of Phase Change Microparticles for Local Heat Transfer Enhancement in Laminar Flows

Andrej Lenert[1], Youngsuk Nam[1,2], Bekir S. Yilbas[3], and Evelyn N. Wang[1]

[1]Device Research Laboratory
Department of Mechanical Engineering
Massachusetts Institute of Technology
Cambridge, MA, USA

[2]Department of Mechanical Engineering
Kyung Hee University
Yongin, Korea

[3]Department of Mechanical Engineering
King Fahd University of Petroleum and Minerals
Dharhan, Saudi Arabia

Corresponding Author:
Evelyn N. Wang
Department of Mechanical Engineering
Massachusetts Institute of Technology
77 Massachusetts Avenue, 3-461B
Cambridge, MA 02139, USA
Tel: 1 (617) 324-3311
Email: enwang@mit.edu

DOI: 10.1016/j.ijheatmasstransfer.2012.09.014

Source: International Journal of Heat and Mass Transfer 56, no. 1–2, p. 380–389, 2013.

Abstract

Phase change material (PCM) suspensions have received wide spread attention for increased thermal storage in various thermal systems such as heat sinks for electronics and solar thermal applications. To achieve further heat transfer enhancement, this paper investigates the effect of focusing micron-sized phase-change particles (PCMs) to a layer near the heated wall of a parallel plate channel. A numerical model for fully-developed laminar flow with a constant heat flux applied to one wall is developed. Melting of the focused PCMs is incorporated using a temperature-dependent effective heat capacity. The effect of channel height, height of the focused PCM stream, heat flux, and fluid properties on the peak local *Nusselt* number (Nu^*) and the averaged *Nusselt* number over the melting length (Nu_{melt}) are investigated. Compared to the thermally-developed *Nusselt* number for this geometry ($Nu_o = 5.385$), Nu_{melt} and Nu^* enhancements of 8% and 19% were determined, respectively. The local heat transfer performance is optimized when the PCMs are confined to within 30% of the channel height. The present work provides an extended understanding of local heat transfer characteristics during melting of flowing PCM suspensions, and offers a new method for enhancing heat transfer performance in various thermal-fluidic systems.

Keywords: Phase-change material (PCM), melting, local heat transfer, focusing, particle distribution, mini/microchannels.

Nomenclature

c_p	Heat capacity [J/kg-K]
d_p	Particle diameter [m]
D_h	Hydraulic diameter (2H for parallel plates) [m]
D_B	Brownian diffusion coefficient [m^2/s]
h_{sf}	Latent heat of PCMs [kJ/kg]
H	Channel height [m or mm]
k	Thermal conductivity [W/m-K]
L_{th}	Thermal entrance length [m]
$\dot{m}$	Mass flow rate [kg/s]
ML	Dimensionless initial subcooling: $(T-T_i)/\Delta T_o$ [-]
Mr	Dimensionless melting temperature range: $\Delta T_{melt}/\Delta T_o$ [-]
Nu	*Nusselt* number [-]
P	Pressure [Pa]
Pe	*Peclet* number: UD_h/α [-]
q''	Heat flux [W/m^2]
Re	*Reynolds* number: $\rho UD_h/\mu$ [-]

DOI: 10.1016/j.ijheatmasstransfer.2012.09.014

Source: International Journal of Heat and Mass Transfer 56, no. 1–2, p. 380–389, 2013.

Ste *Stefan* number: $\frac{c_{p,f}}{\omega h_{sf} / \Delta T_o}$ [-]

Ste_m Modified *Stefan* number: $\frac{c_{p,f}}{\omega h_{sf} / \Delta T_{melt}}$ [-]

T Temperature [K]

t Time [s]

u Local velocity [m/s]

U Mean fluid velocity [m/s]

x,y Coordinates [m]

*x** Dimensionless position: $x/D_h Pe$ [-]

Greek Symbols

α Thermal diffusivity ($k/\rho c_p$) [m^2/s]

δ Height of the phase-change stream [m]

δ_B PCM Brownian diffusion distance [m]

μ Viscosity [Pa·s]

ρ Density [kg/m^3]

ϕ PCM-particle volume fraction [-]

ω PCM-particle mass fraction: $\rho_p \phi / \rho_{eff}$ [-]

Superscript

* Local maximum

min Minimum

\- Onset of melting

\+ End of melting

Subscripts

b Bulk

δ Pertaining to phase-change stream

eff Effective property of PCM suspension

f Fluid medium

i Inlet

melt Averaged over PCM melt region

o Thermally-developed

p Particle (outside of melt region)

DOI: 10.1016/j.ijheatmasstransfer.2012.09.014

Source: International Journal of Heat and Mass Transfer 56, no. 1–2, p. 380–389, 2013.

w Heated wall

x Local

1. Introduction

When suspended in a heat transfer fluid, PCMs serve to increase the effective heat capacity of a fluid over a relatively small temperature range as the core undergoes melting (*i.e.*, phase change). Since thermal systems are operated with a limited temperature difference between inlet and outlet, the enhancement of effective heat capacity resulting from the latent heat of fusion increases the energy storage density. Consequently, either thermal performance is improved or the pumping power requirement may be reduced.

Previous studies have developed numerical models to understand the hydrodynamic and heat transfer characteristics of PCM suspensions (*i.e.*, slurries). A review by Dutil *et al*. focuses on numerical studies modeling convective heat transfer in PCM suspensions with summaries of methods, model validation steps and main contributions [1]: while, Zhang *et al.* summarizes work addressing material properties and applications of PCM suspensions [2]. Most of the numerical studies model the slurry as a bulk fluid using the effective heat capacity model [3-9] originally introduced by Alisetti *et al.* [3]. Alternative approaches treat the latent heat as an additional source term representing the absorbed heat during the phase change process in the PCM [10, 11], or describe the carrier fluid and the PCM phases using separate conservation equations with appropriate interaction terms [12].

Experiments have also been conducted to evaluate the heat transfer characteristics of PCM suspensions [13-23]; results from forced convection, constant heat flux experiments with suspensions of microencapsulated PCM particles show the effects of the following: *Stefan* number, PCM mass fraction, flow rate, flow regime, inlet temperature subcooling, and particle size. Thermal performance tends to increase as the mass fraction increases, but the optimal mass fraction balances both the heat transfer enhancement and the pumping power increase [15, 16, 23]. To improve the effective thermal conductivity of slurries, investigators have studied hybrid suspensions of alumina nanoparticles and PCMs [21, 22]; however, experiments showed that the viscosity of hybrid suspensions is anomalously high, exceeding enhancements in heat transfer.

Although previous work has focused on enhancing overall thermal performance using PCM suspension fluids, certain studies have also considered the effects of PCM suspensions on the local heat transfer characteristics. Local heat transfer coefficient variations along the axial direction (h_x) have been reported using both numerical models [8, 9] and in experiments [17-19]. Sabbah *et al.* showed that h_x increases when the melting interface is near the heated wall and decreases when the interface moves toward the tube center [9]. Meanwhile, Zeng *et al.* investigated the effects of the *Stefan* number (*Ste*), the PCM melting range (*Mr*), the flow rate, and the particle diameter on the local heat transfer characteristics; the amplitude of the h_x variation was observed to increase with decreasing *Ste* and decreasing *Mr*, which were the dominant parameters in the study. Furthermore, Wang *et al.* demonstrated local heat transfer enhancements as high as 60% compared to the basefluid and suggested a heat transfer correlation to predict the average heat transfer

DOI: 10.1016/j.ijheatmasstransfer.2012.09.014

Source: International Journal of Heat and Mass Transfer 56, no. 1–2, p. 380–389, 2013.

coefficient during PCM melting [18, 19]. The effects of PCMs on local heat transfer, however, have not been investigated in detail beyond these studies. In particular, understanding the influence of the distribution of PCM particles inside the channel and how it can be used to achieve further heat transfer enhancements was not considered in previous work.

In this paper, we investigated the effect of focusing micron-sized PCMs to a layer near the heated wall on local heat transfer coefficient. Various techniques have been used to focus, separate and sort microparticles demonstrating the feasibility of the proposed concept, including: pinched flows (*e.g.,* [24]), where flow asymmetries are used to separate particles; inertial focusing, where particles migrate away from the channel center and walls generating continuous particle streams due to inertial lift forces (*e.g.,* [25]); magnetophoresis (*e.g.,* [26]), where magnetic particles are manipulated using an externally applied magnetic field; and acoustophoresis (*e.g.,* [27]), where particles are driven towards minima of an acoustic force field acting perpendicular to the flow direction due to density and compressibility contrast compared with the basefluid. The effect of focusing particles on heat transfer, however, has not been investigated. A numerical model is developed which assumes fully-developed laminar flow and a constant heat flux applied to one wall. Melting of the focused phase-change particles is incorporated in the model using a temperature-dependent effective heat capacity. Using near-wall PCM focusing, we report increases in the averaged and peak *Nusselt* numbers.

2. Model Formulation

We developed a two-dimensional model (*x,y*) of laminar flow between parallel plates to investigate the effect of focusing PCMs near a heated wall. Constant heat flux (*q"*) is applied to the bottom wall, while the top wall is adiabatic. As shown in Figure 1, PCMs are confined to a layer near the bottom wall (δ) which is a fraction of the total channel height (*H*). Pure fluid and PCM streams are introduced upstream such that the flow is assumed to be hydrodynamically fully-developed by the time it reaches the heated region. The inlet temperature is uniform and well below the onset of melting (*i.e., ML* >> 1). Melting of the PCMs in the phase-change stream is modeled using a temperature-dependent effective heat capacity.

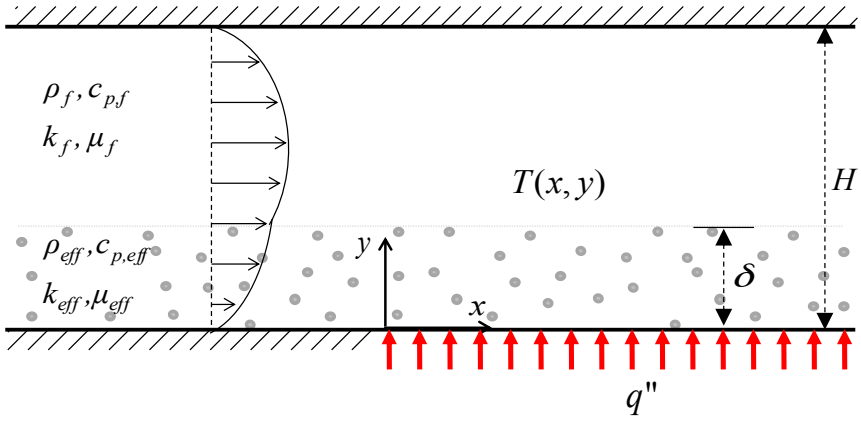

Figure 1: Schematic for model formulation of a 2-D parallel plate channel with fully-developed flow and PCMs confined to a layer (δ) near the heated bottom wall.

DOI: 10.1016/j.ijheatmasstransfer.2012.09.014
Source: International Journal of Heat and Mass Transfer 56, no. 1–2, p. 380–389, 2013.

In modeling this system, we make the following simplifications in order to focus on the effect of the PCMs:

- Local temperature differences between the PCMs and the surrounding fluid are neglected. This assumption is consistent with bulk fluid treatments [3-6, 8] and was justified for PCMs on the order of a micron [5].
- Temperature dependence of the pure fluid material properties is neglected over the relatively small melting range.
- Differences in the properties of the solid and the post-melting phase of the PCMs are neglected.
- The encapsulating/stabilizing shell is assumed to be negligibly thin compared to the phase-changing core.
- Axial heat conduction and viscous dissipation are neglected.
- The PCM suspension is considered Newtonian.
- PCMs are homogenously distributed throughout the phase-change stream.
- Diffusion of PCMs from the phase-change stream is neglected since it is small relative to the channel height (see Appendix A.3).

2.1 Effective Suspension Properties

In this study, the thermophysical properties of the PCM suspensions are described using effective models. The following models hold for spherical, non-agglomerating, micron-sized particles with volume fractions up to ~20%.

Density

Considering a simple mechanical mixture of components [28], the effective density of the PCM suspension is equal to:

$$\rho_{eff} = (1-\phi)\rho_f + \phi\rho_p \tag{1}$$

where ϕ is the particle volume fraction in the PCM stream.

Heat Capacity

The effective heat capacity is represented by a half-period sinusoidal function:

$$c_{p,eff} = (1-\omega^{\delta})c_{p,f} + \omega^{\delta}\left\{c_{p,p} + \frac{\pi}{2}\left(\frac{h_{sf}}{\Delta T_{melt}} - c_{p,p}\right)\sin\left(\pi\frac{T-T^{-}}{\Delta T_{melt}}\right)\right\} \tag{2}$$

where ω^{δ} is the particle mass fraction inside the PCM stream, h_{sf} is the latent heat of PCMs, T^{-} is the temperature at the onset of melting, and ΔT_{melt} (= T^{+}-T^{-}) is the melting range. This formulation is consistent with previous effective heat capacity models [3-6, 8].

Thermal Conductivity

Maxwell's effective theory [29] is used to calculate the thermal conductivity of the suspension:

DOI: 10.1016/j.ijheatmasstransfer.2012.09.014

Source: International Journal of Heat and Mass Transfer 56, no. 1–2, p. 380–389, 2013.

$$\frac{k_{eff}}{k_f} = \frac{2 + k_p/k_f + 2\phi(k_p/k_f - 1)}{2 + k_p/k_f - \phi(k_p/k_f - 1)} \tag{3}$$

This relation agrees with experimental results for spherical microparticles with volume fractions up to 22% [13]. Microconvection-related enhancements discussed in studies considering larger particles are neglected in this study since they scale with d_p [30]; results from previous studies indicate these effects are negligible for micro/nanoparticles compared to the effects of phase change [10, 13, 17].

Viscosity

The dependence of the effective viscosity (μ_{eff}) of the PCM stream on the volume fraction of particles is computed using Vand's [31] semi-empirical model:

$$\frac{\mu_{eff}}{\mu_f} = (1 - \phi - 1.16\phi^2)^{-2.5} \tag{4}$$

This model holds for non-interacting, hard, uncharged particles and agrees with experimental results for spherical microparticles ($d_p > 0.3$ μm) with volume fractions up to 20% [13]. Although several researchers have suggested higher enhancement coefficients by fitting their experimentally-measured viscosity (*e.g.*, [18]), Vand's model has been predominantly used in previous PCM studies (*e.g.*, [5, 6, 13]).

2.2 Governing Equations

Under the above assumptions, the momentum and energy equations for fully-developed laminar flow inside asymmetrically-heated parallel plates with a spatial and temperature dependent specific heat, simplify to the following:

$$\frac{\partial}{\partial y}\left[\mu(y)\frac{\partial u}{\partial y}\right] = \frac{dP}{dx} \tag{5}$$

$$\rho(y)c_p(y,T)u(y)\frac{\partial T}{\partial x} = \frac{\partial}{\partial y}\left[k(y)\frac{\partial T}{\partial y}\right] \tag{6}$$

Eq. 5, along with no-slip boundary conditions, is solved analytically in Appendix A.1 to determine the velocity profile ($u(y)$) which is incorporated into the energy equation. Numerical methods for solving Eq. 6, along with the appropriate boundary conditions, are described and validated in Appendix A.

DOI: 10.1016/j.ijheatmasstransfer.2012.09.014

Source: International Journal of Heat and Mass Transfer 56, no. 1–2, p. 380–389, 2013.

3. Results and Discussion

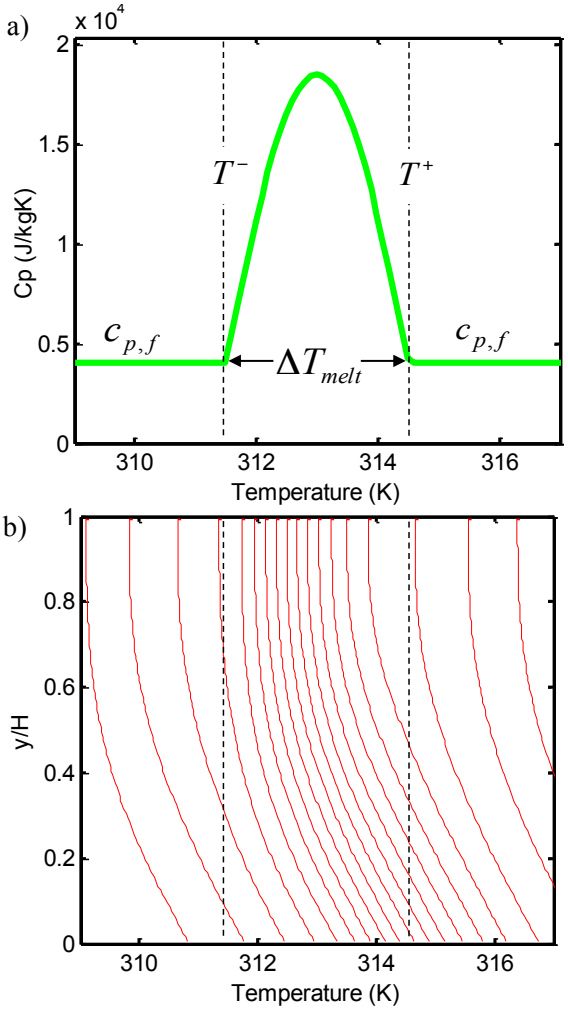

Figure 2: a) Effective heat capacity of the PCM suspension as a function of temperature. b) Temperature profiles at regularly spaced intervals (1.7 mm) along the axial direction of the channel. The melting range (ΔT_{melt}) is bound by T- and T+, represented by the region between the dashed lines (U = 5 mm/s, q"= 5 kW/m^2, H = 0.5 mm, δ/H = 1, ΔT_{melt} = 3 K, ωh_{sf} = 30 kJ/kg, k = 0.624 W/mK, ρ = 992 kg/m^3, $c_{p,f}$ = 4067 J/kgK).

In this section, we explore the effects of various geometrical and material parameters on the features of the local *Nusselt* number (Nu_x):

$$Nu_x = \frac{q'' D_H}{k_f (T_{w,x} - T_{b,x})} \tag{7}$$

where D_H is the hydraulic diameter (=2H), k_f is the thermal conductivity of the pure fluid, $T_{w,x}$ is the local wall temperature, and $T_{b,x}$ is the local bulk temperature:

DOI: 10.1016/j.ijheatmasstransfer.2012.09.014

Source: International Journal of Heat and Mass Transfer 56, no. 1–2, p. 380–389, 2013.

$$T_{b,x} = \frac{\int_0^H \rho(y) c_p(y,T) U(y)\, T dy}{\int_0^H \rho(y) c_p(y,T) U(y)\, dy} \tag{8}$$

The local heat transfer coefficient profile is rationalized using simple physical arguments in Section 3.1. Based on this understanding, the effect of focusing the PCMs near the heated wall is explained (Section 3.2). The effects of the PCM-particle mass fraction (ω), mean fluid velocity (U), channel height (H), and heat flux (q'') on Nu_x are explored in Section 3.3, and the results are summarized using three dimensionless groups (Section 3.4).

To isolate the effects of phase change and particle focusing, the effect of the PCMs on the suspension properties (except for $c_{p,eff}$ during melting) are assumed to be negligible in Sections 3.1-3.4. A physically realistic case is discussed in Section 3.5 which includes the parasitic effects associated with the dependence of the effective thermal conductivity and viscosity on the addition of PCMs.

3.1 Nu_x Profile

To illustrate the local heat transfer behavior during melting of a flowing PCM suspension, we present the case of PCMs (h_{sf} = 150 kJ/kg) suspended in water (k_f = 0.624 W/mK, $c_{p,f}$ = 4067 J/kgK, ρ_f = 992 kg/m^3, μ_f = 6.36·10^{-4} Pa·s) with q'' = 5 kW/m^2, U = 5 mm/s , and H = 0.5 mm. These parameters represent a low heat-flux case with Re numbers characteristic of laminar flows in micro/minichannels and high enough Pe numbers (>10) for axial conduction to be negligible.

First, we consider the case when the PCMs are uniformly distributed across the height of the channel (*i.e.,* $\delta = H$) with a mass fraction of 0.20, and assumed to melt across a 3 K temperature range (ΔT_{melt} = 3K) centered about 313 K. The effective heat capacity of the suspension is shown in Figure 2a.

Figure 2b shows the temperature profiles of the fluid as it traverses the melting region. The increased effective specific heat over the melting region has the effect of slowing down the rate of temperature rise locally. This observation is explicit in Figure 3a where the rate of change of temperature with respect to the axial distance (x) is much lower where the PCMs are melting.

However, the fluid near the heated wall is the first to enter and exit the melting region as shown in Figure 2b. This movement of the melting interface away from the heated wall leads to maxima and minima in the local heat transfer as shown in Figure 3b. Similar effects on the local heat transfer have been observed in previous studies (*e.g.*, [8, 9, 17-19]).

The shape of Nu_x can be more quantitatively understood by partitioning the melting range into the four sub-regions (*i-iv*) shown in Figure 3b.

DOI: 10.1016/j.ijheatmasstransfer.2012.09.014

Source: International Journal of Heat and Mass Transfer 56, no. 1–2, p. 380–389, 2013.

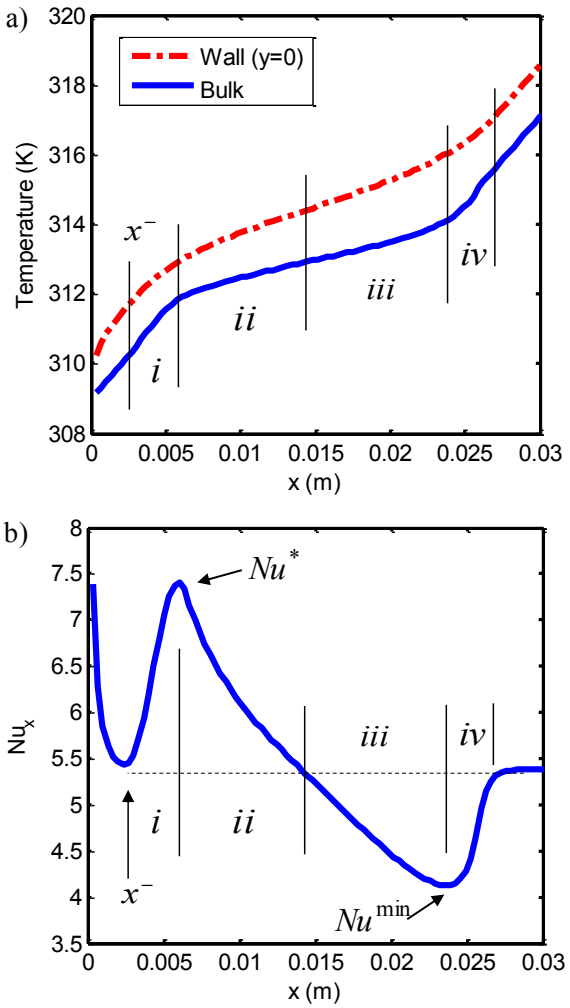

Figure 3: a) Bulk and wall temperatures as a function of length (*x*) showing a decrease in rate of temperature rise inside melting region and b) local *Nusselt* number as a function of length (*x*). Melting region divided into sub-regions (*i-iv*) to clarify thermal behavior (same parameters as Figure 2 were used).

Sub-region (i):

This sub-region is bound by the onset of melting (x^-) and the maximum local heat transfer coefficient (Nu^*). At x^-, the temperature difference between the wall and the bulk is:

$$\Delta T_o \equiv T_{w,x^-} - T_{b,x^-} = \frac{q'' D_H}{Nu_o k} \tag{9}$$

However, as the fluid near the wall enters the phase-change region, its rate of change of temperature decreases with respect to the bulk. To understand this effect, the local heat transfer coefficient is rewritten in terms of the temperatures at the onset of melting (x^-) and their respective linearized rates of temperature rise as a function of x:

$$h_x \approx \frac{q''}{\Delta T_o - (x - x^-)\left(\frac{\partial T_b}{\partial x} - \frac{\partial T_w}{\partial x}\right)} \tag{10}$$

DOI: 10.1016/j.ijheatmasstransfer.2012.09.014

Source: International Journal of Heat and Mass Transfer 56, no. 1–2, p. 380–389, 2013.

When $\partial T_b / \partial x > \partial T_w / \partial x$, there is an enhancement in the heat transfer coefficient. For the purpose of this simple treatment, we assume that the rate of change of temperature is constant in each sub-region and can be approximated using the rate of change for the thermally-developed case:

$$\frac{\partial T_b}{\partial x} \approx \frac{q''}{\dot{m} c_{p,f}} \tag{11a}$$

$$\frac{\partial T_w}{\partial x} \approx \frac{q''}{\dot{m}(\omega h_{sf} / \Delta T_{melt})} \tag{11b}$$

Since the rate of temperature rise at the wall (Eq. 11b) is inversely proportional to the effective heat capacity during melting of the PCMs ($\omega h_{sf}/\Delta T_{melt}$), it is indeed smaller than the rate of temperature rise of the bulk (Eq. 11a). Thus, the temperature difference between the wall and the bulk diminishes over the length of *sub-region (i)*, leading to a maximum (Nu^*). We approximate the axial length of this sub-region (Δx_i) by the distance needed for the bulk temperature to reach the original wall temperature ($T_{w,x-}$) at a constant rate of temperature rise:

$$\Delta x_i \approx \frac{\Delta T_o}{\partial T_b / \partial x} = \frac{\dot{m} c_{p,f} D_H}{Nu_o k} \tag{12}$$

Sub-region (ii):

The beginning of this sub-region coincides with Nu^*. At this point, the difference between the wall and bulk temperatures is at a minimum. The bulk and wall regions have approximately the same effective heat capacity ($\omega h_{sf}/\Delta T_{melt}$) since the fluid is inside the melting region; hence, the temperature profile re-develops to its pre-melting shape. By analogy with the thermal entrance length (L_{th}), the length of this region is proportional to the *Pe* number (and in turn, the effective heat capacity):

$$\Delta x_{ii} \approx Pe_{melt} D_H \propto \omega h_{sf} / \Delta T_{melt} \tag{13}$$

As compared to the inlet, the thermally diffusivity in *sub-region (ii)* is relatively low because of the high effective heat capacity; this explains why Δx_{ii} is significantly longer than the thermal entrance length.

Sub-region (iii):

This sub-region begins with a developed profile inside the melt region and ends with the minimum local *Nusselt* number (Nu^{min}). The sub-region is physically similar to *sub-region (i)*, except that the specific heat of the wall and the bulk regions are interchanged. The fluid near the wall exits the melting region while the bulk of the fluid remains in the region, amplifying the temperature difference and leading to deterioration of the local heat transfer. By analogy with *sub-region (i)*, we determine that the length of *sub-region (iii)* is proportional to $\omega h_{sf}/\Delta T_{melt}$:

DOI: 10.1016/j.ijheatmasstransfer.2012.09.014

Source: International Journal of Heat and Mass Transfer 56, no. 1–2, p. 380–389, 2013.

$$\Delta x_{iii} \approx \frac{\dot{m}(\omega h_{sf}/\Delta T_{melt})D_H}{Nu_o k} \tag{14}$$

Since $\omega h_{sf}/\Delta T_{melt} > c_{p,f}$, Δx_{iii} is longer than Δx_i, as evident in Figure 3b.

Sub-region (iv):

The final sub-region occurs at the exit of the melting region. It begins at the location of Nu^{min}, where the temperature difference between the wall and bulk is at a maximum. The fully-developed temperature profile re-establishes itself over the course of this sub-region.

Its length (Δx_{iv}) is proportional to the thermal entrance length (L_{th}), and thus shorter than (Δx_{ii}):

$$\Delta x_{iv} \approx PeD_H \propto c_{p,f} \tag{15}$$

Although the above treatment is approximate, it rationalizes the basic features of the local heat transfer and will aid in explaining the effect of focusing PCMs near the heated wall.

3.2 Effect of PCM Focusing

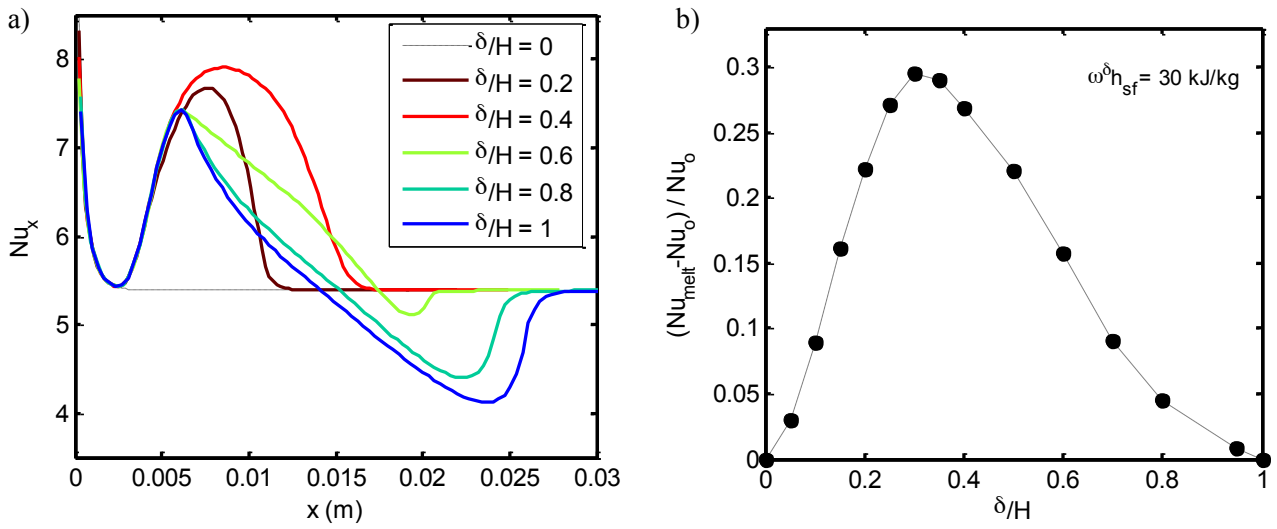

Figure 4: a) Local *Nusselt* number (Nu_x) and b) *Nusselt* number averaged over the melting region (Nu_{melt}) for δ/H ranging from 0-1. The mass fraction inside the phase-change stream is kept constant ($\omega^{\delta}h_{sf}$= 30 kJ/kg, U = 5 mm/s, q"= 10 kW/m^2, H = 1 mm, ΔT_{melt} = 3 K, k = 0.624 W/mK, ρ = 992 kg/m^3, $c_{p,f}$= 4067 J/kgK).

The effect of the PCM stream height as a fraction of the channel height is shown in Figure 4a. As δ decreases, the deterioration of the local heat transfer vanishes since regions of complete near-wall melting with incomplete melting in the bulk (associated with *sub-regions iii-iv*) are eliminated. Thus, the Nu_x degradation can be circumvented by focusing the PCMs near the heated wall. For cooling applications, eliminating the degradation of Nu_x near the channel exit is desirable for hot-spot prevention (*i.e.,* to minimize the absolute temperature of the wall near the channel exit).

DOI: 10.1016/j.ijheatmasstransfer.2012.09.014

Source: International Journal of Heat and Mass Transfer 56, no. 1–2, p. 380–389, 2013.

In other applications, the average *Nusselt* number over the entire melting region (Nu_{melt}) could be important if it is desired that the PCMs melt fully (*i.e.,* for improved thermal storage). If the mass fraction of PCMs in the phase-change stream (ω^{δ}) is kept constant as δ/H decreases, then Nu_{melt} has a distinct peak (29% enhancement) when δ/H is approximately 0.30, as shown in Figure 4b. $\delta/H \approx 0.30$ was in general found to optimize Nu_{melt} in this geometry (*i.e.*, asymmetrical heating between parallel plates with fully-developed flow).

3.3 Parametric Study

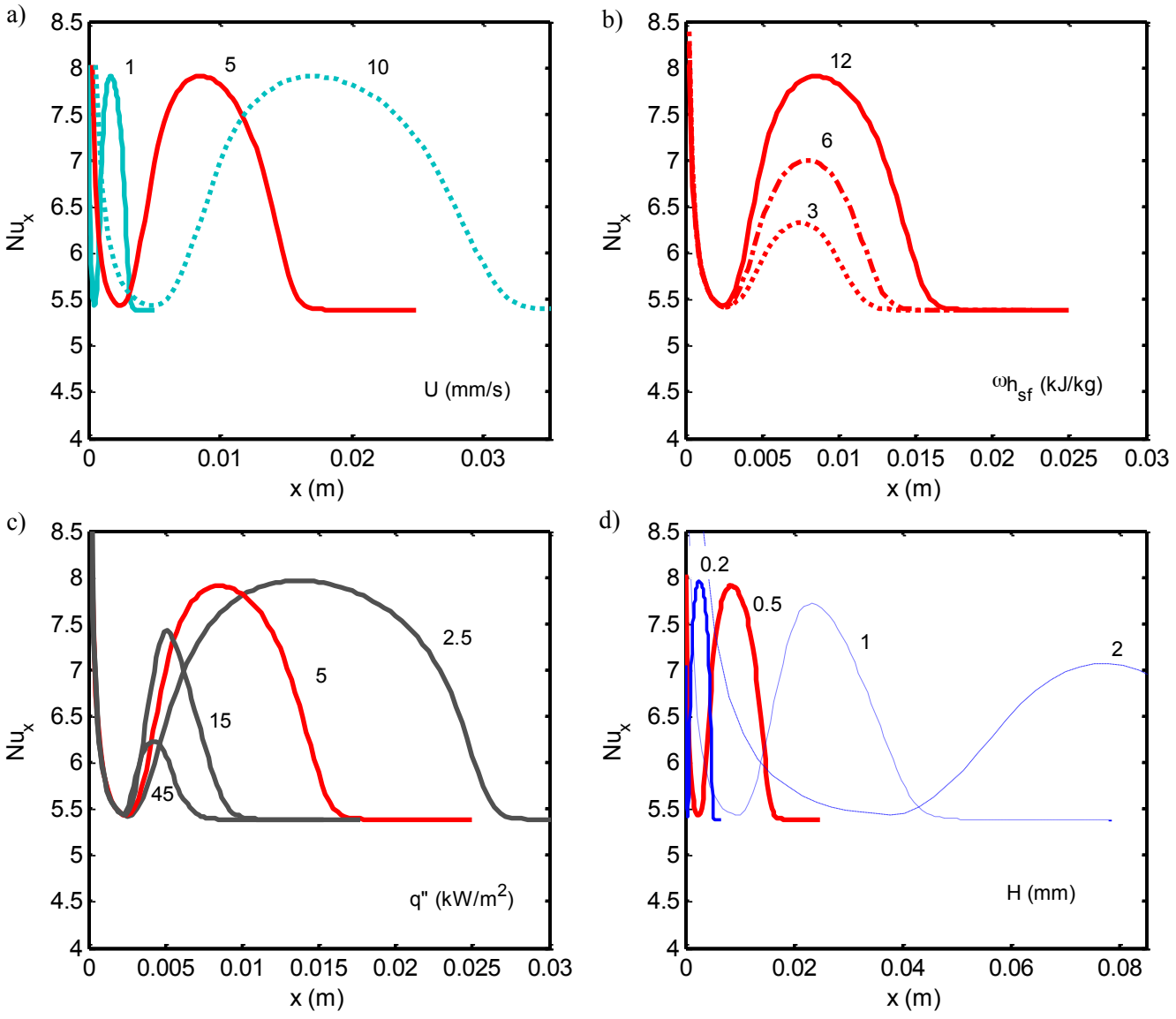

Figure 5: Parametric study of Nu_x for variable latent heat and heat flux: a) U ranging from 1 to 10 mm/s, b) ωh_{sf} ranging from 3 to 12 kJ/kg, c) q'' ranging from 2.5 to 45 kW/m^2, and d) H ranging from 0.2 to 2 mm. The baseline in all of the graphs (solid red) shows the case when U = 5 mm/s, q''= 5 kW/m^2, H = 0.5 mm, δ/H = 0.4, ΔT_{melt} = 3 K, ωh_{sf}= 12 kJ/kg, k = 0.624 W/mK, ρ = 992 kg/m^3, $c_{p,f}$= 4067 J/kgK.

DOI: 10.1016/j.ijheatmasstransfer.2012.09.014

Source: International Journal of Heat and Mass Transfer 56, no. 1–2, p. 380–389, 2013.

In this section, we explore the effects of velocity (U), latent heat (ωh_{sf}), heat flux (q'') and channel height (H) on the features of Nu_x. The baseline for this parametric study (solid red in Figure 5) shows the case when $U = 5$ mm/s, $q'' = 5$ kW/m^2, $H = 0.5$ mm, $\delta/H = 0.4$, $\Delta T_{melt} = 3$ K, $\omega h_{sf} = 12$ kJ/kg.

The velocity of the fluid (U) prolongs the length of the melt region, as shown in Figure 5a. Nevertheless, it is interesting to note that changes in velocity have no impact on the magnitude of Nu^*.

The total mass fraction of PCMs ($\omega = \omega^{\delta}\ \delta/H$) and the heat of fusion (h_{sf}) have a significant influence on the magnitude of heat transfer enhancement since they increase the effective heat capacity during melting. Figure 5b shows that the enhancement increases with increasing amount of latent heat in the channel.

The effect of heat flux (q'') on Nu_x is shown in Figure 5c. As the heat flux is increased above a threshold value (~5 kW/m^2 in this case), the magnitude of heat transfer enhancement decreases. Below this threshold value, however, the heat flux has little effect on Nu^*.

Although not as apparent as with q'', the height (H) of the channel displays a similar effect as shown in Figure 5d: increasing H has a negligible effect for small H values, but Nu^* decreases as H increases beyond a threshold value. The results of Figures 5c and 5d suggest the existence of two regimes: a low ΔT_o (low profile curvature) regime and a high ΔT_o (high profile curvature) regime. The following section will explore this observation further.

3.4 Dimensionless Groups

Dimensionless groups are presented to generalize the trends discussed above. When the model is simplified to isolate for the effect of phase-change, the following dimensionless groups are relevant: Ste (and Ste_m), a ratio of sensible to latent heat; δ/H, a ratio of the PCM-particle stream height to the channel height; and $\Delta T_{melt}/\Delta T_o$, a ratio of the melting temperature range to the thermally-developped temperature difference between the wall and the bulk (typically referred to as Mr):

$$Ste = \frac{c_{p,f}}{\omega h_{sf} / \Delta T_o} \tag{16}$$

$$\frac{\delta}{H} \tag{17}$$

$$Mr = \frac{\Delta T_{melt}}{\Delta T_o} \tag{18}$$

According to Figure 6a, Nu^* generally decreases as Mr increases but with two distinct slopes. This confirms the existence of two regimes, as suggested in the previous section. When $Mr<1$, the profile curvature does not have a significant effect on Nu^*. When $Mr>1$, however, increasing the heat flux or the channel height results in lowering of the heat transfer enhancement.

DOI: 10.1016/j.ijheatmasstransfer.2012.09.014

Source: International Journal of Heat and Mass Transfer 56, no. 1–2, p. 380–389, 2013.

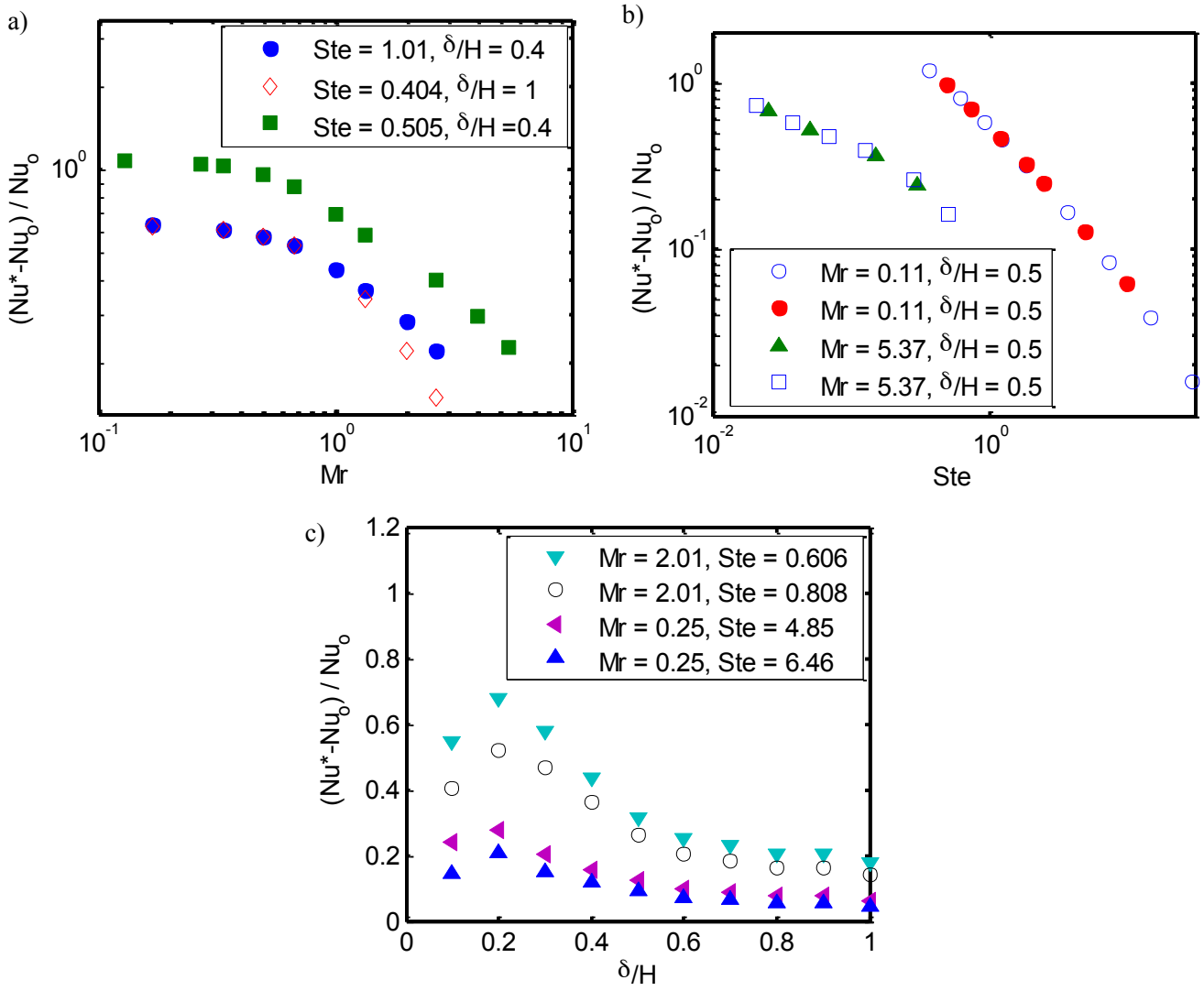

Figure 6: *Nu with respect to the following dimensionless groups: a) Mr, ranging from 0.1 to 10 (ΔT_{melt} varied), b) *Ste,* ranging from 0.01 to 30 ($c_{p,f}$ and h_{sf} varied), c) *δ/H* ranging from 0 to 1 (*q"*, *δ*, *H* varied).**

The existence of these two regimes is also apparent in the Nu^* dependency on the *Ste* (Figure 6b). In both regimes, as the ratio of latent to sensible heat increases (decreasing *Ste*), the enhancement in heat transfer is augmented. However, the enhancement scales differently depending on the regime: the effect of *Ste* is more significant when $Mr < 1$.

Finally, the ratio of the PCM stream height to the channel height is shown in Figure 6c, where the total mass fraction ($\omega = \omega^{\delta}\ \delta/H$) was kept constant (such that *Ste* = const.) by increasing ω^{δ} to counteract the decrease in δ/H. In general, Nu^* increases as the PCMs are focused closer to the heated wall up to $\delta/H \sim 0.25$, at which point focusing the PCMs becomes detrimental. This reduction in Nu^* is most likely attributed to the increasing importance of heat conduction between the focused stream and the pure-fluid at small δ scales, which increases the wall temperature regardless of the phase-change.

Within the specified limits, results of this study are summarized in the form of correlations relating Nu^* to the three dimensionless groups presented:

DOI: 10.1016/j.ijheatmasstransfer.2012.09.014

Source: International Journal of Heat and Mass Transfer 56, no. 1–2, p. 380–389, 2013.

$$\frac{Nu^* - Nu_o}{Nu_o} = 0.214 Ste^{-0.86} Mr^{-0.08} \left(\frac{\delta}{H}\right)^{-1} \qquad [Mr < 1,\ 0.3 < \frac{\delta}{H} \le 1] \qquad (19)$$

$$\frac{Nu^* - Nu_o}{Nu_o} = 0.208 Ste_m^{-0.44} Mr^{-0.156} \left(\frac{\delta}{H}\right)^{-1} \qquad [Mr > 1,\ 0.3 < \frac{\delta}{H} \le 1] \qquad (20)$$

Results from 157 unique simulations were fit to obtain the above expressions (see Appendix B). In Eq. 20, defining the *Stefan* number with respect to ΔT_{melt} (as opposed to T_o) improves the quality of the fit significantly, indicating the dominance of ΔT_{melt} in the $Mr > 1$ regime. The coefficient of determination (R^2) for Eq. 19 and Eq. 20 is 0.99 and 0.86, respectively.

3.5 Parasitic effects

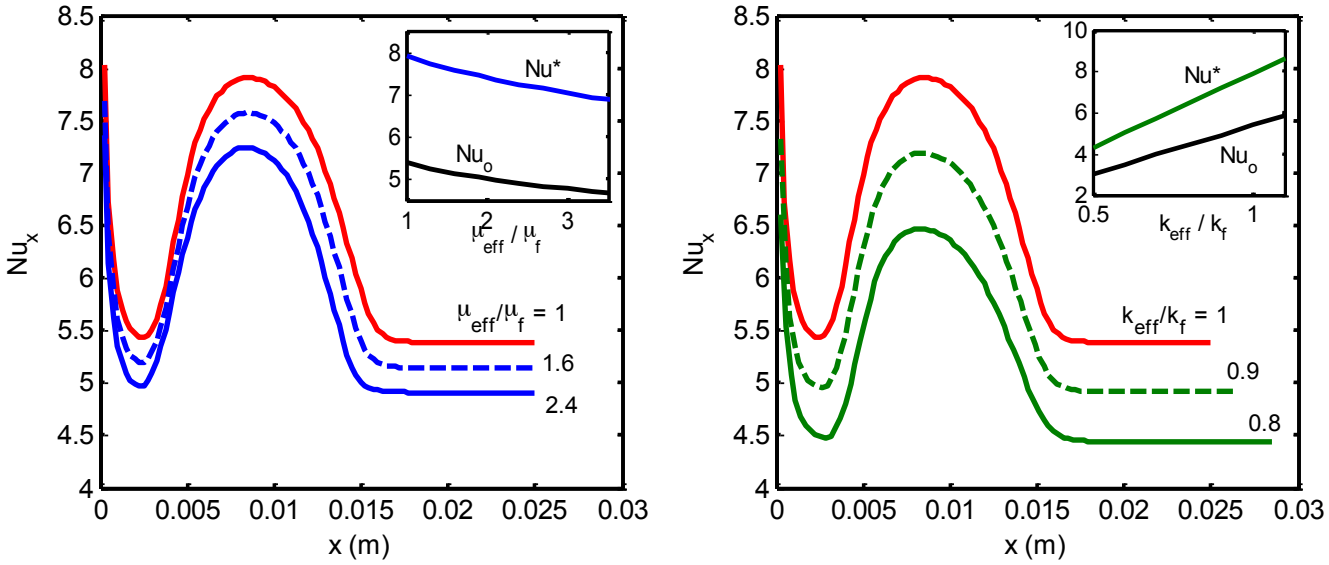

Figure 7: Parasitic effects on Nu_x due to a) increased viscosity (μ_{eff}) and b) decreased thermal conductivity (k_{eff}) of the focused PCM stream. The baseline in all of the graphs (solid red) shows the case when U = 5 mm/s, q"= 5 kW/m^2, H = 0.5 mm, δ/H = 0.4, ΔT_{melt} = 3 K, ωh_{sf} = 12 kJ/kg, k = 0.624 W/mK, ρ = 992 kg/m^3, $c_{p,f}$ = 4067 J/kgK.

It is well known that the addition of PCMs increases the viscosity of fluids and may degrade the overall heat transfer performance. Although the overall pressure drop may be reduced by focusing the PCM particles (compared to the $\delta/H = 1$ case), the presence of a higher viscosity fluid near the heated wall distorts the velocity profile and decreases the local heat transfer performance. The degradation of Nu_x scales approximately linearly with the viscosity ratio of the two streams (μ_{eff}/μ_f), as shown in Figure 7a.

Similarly, the effective thermal conductivity of the focused stream typically decreases with the addition of PCM particles which further degrades Nu_x as compared to the original pure fluid performance (note: the definition of Nu_x is written with respect to k_f for consistency). As shown in Figure 7b, Nu_x also scales approximately linearly with the thermal conductivity ratio of the two streams (k_{eff}/k_f).

DOI: 10.1016/j.ijheatmasstransfer.2012.09.014

Source: International Journal of Heat and Mass Transfer 56, no. 1–2, p. 380–389, 2013.

Considering the non-negligible nature of these parasitic effects at higher volume fractions, we relax the assumptions of Sections 3.1-3.4 and re-evaluate the idealized enhancements presented in Section 3.2 based on mePCM property data measured by Zeng *et al.* [8]: k_p = 0.211 W/mK, $c_{p,p}$ = 1609 J/kgK, ρ_p = 1045 kg/m^3. All other parameters are kept the same (*i.e.*, δ/H=0.30, ω^{δ} = 0.20, h_{sf} = 150 kJ/kg, water, *etc*.) such that: ϕ = 0.192, ρ_{eff}/ρ_f = 1.01 (Eq. 1), k_{eff}/k_f = 0.845 (Eq. 3), and μ_{eff}/μ_f = 1.952 (Eq. 4). In this case, Nu^* and Nu_{melt} enhancements of 18.6% and 7.9% were obtained, respectively.

Although lower than the idealized results of Section 3.2, this result represents an un-optimized enhancement of local heat transfer within the bounds of applicability of the physical models and simplifying assumptions described in Section 2. In future work, application-dependent optimization should be investigated. Also, correction factors may be appended to Eqs. 19-20 to include the parasitic effects based on measured or predicted properties.

4. Conclusions

The effect of focusing micron-sized phase-change particles to a layer near the heated wall of a parallel plate channel was investigated. A numerical model was developed which models melting of the PCMs using a spatially-dependent and temperature-dependent effective heat capacity. In the unfocused case, the melting region was divided into four sub-regions based on the major features of the local *Nusselt* number profile, including the local peak (Nu^*) and minimum (Nu^{min}) *Nusselt* numbers. Deterioration of the local heat transfer (*i.e.*, Nu^{min}) associated with complete near-wall melting with incomplete melting in the bulk is eliminated when PCMs are focused to a region near the heated wall. A parametric study shows that Nu^* increases with increasing particle mass fraction and latent heat as well as with decreasing melting range, channel height and heat flux. The existence of two regimes depending on *Mr* was observed and the results were summarized using four dimensionless quantities (*Ste*, Ste_m, δ/H and *Mr*). The averaged *Nusselt* number over the melting length (Nu_{melt}) and Nu^* are both optimized when the PCMs are focused to within 30% of the channel closest to the heated wall. For a physically realistic case, Nu_{melt} and Nu^* enhancements of 8% and 19% were obtained, respectively. These studies suggest a new strategy to enhance heat transfer with phase change particles for cooling and solar thermal applications.

Acknowledgments

The authors would like to thank the King Fahd University of Petroleum and Minerals in Dhahran, Saudi Arabia, for funding the research reported in this paper through the Center for Clean Water and Clean Energy at MIT and KFUPM under PROJECT NUMBER 6918351. Andrej Lenert acknowledges the support of the MIT Energy Initiative and the National Science Foundation GRF.

DOI: 10.1016/j.ijheatmasstransfer.2012.09.014

Source: International Journal of Heat and Mass Transfer 56, no. 1–2, p. 380–389, 2013.

References

1. Dutil, Y., et al., *A review on phase-change materials: Mathematical modeling and simulations.* Renewable and Sustainable Energy Reviews, 2010. **15**(1): p. 112.
2. Zhang, P., Z.W. Ma, and R.Z. Wang, *An overview of phase change material slurries: MPCS and CHS.* Renewable and Sustainable Energy Reviews, 2010. **14**(2): p. 598-614.
3. Alisetti, E.L. and S.K. Roy, *Forced Convection Heat Transfer to Phase Change Material Slurries in Circular Ducts.* Journal of Thermophysics and Heat Transfer., 2000. **14**: p. 115.
4. Hu, X. and Y. Zhang, *Novel insight and numerical analysis of convective heat transfer enhancement with microencapsulated phase change material slurries: laminar flow in a circular tube with constant heat flux.* International Journal of Heat and Mass Transfer, 2002. **45**(15): p. 3163.
5. Kuravi, S., et al., *Numerical Investigation of Flow and Heat Transfer Performance of Nano-Encapsulated Phase Change Material Slurry in Microchannels.* Journal of Heat Transfer, 2009. **131**(6): p. 062901.
6. Zhang, Y., X. Hu, and X. Wang, *Theoretical analysis of convective heat transfer enhancement of microencapsulated phase change material slurries.* Heat and Mass Transfer, 2003. **40**(1): p. 59.
7. Zhao, Z., R. Hao, and Y. Shi, *Parametric Analysis of Enhanced Heat Transfer for Laminar Flow of Microencapsulated Phase Change Suspension in a Circular Tube with Constant Wall Temperature.* Heat Transfer Engineering, 2008. **29**(1): p. 97-106.
8. Zeng, R., et al., *Heat transfer characteristics of microencapsulated phase change material slurry in laminar flow under constant heat flux.* Applied Energy, 2009. **86**(12): p. 2661.
9. Sabbah, R., J. Seyed-Yagoobi, and S. Al-Hallaj, *Heat Transfer Characteristics of Liquid Flow With Micro-Encapsulated Phase Change Material: Numerical Study.* Journal of Heat Transfer, 2011. **133**(12): p. 121702.
10. Charunyakorn, P., S. Sengupta, and S.K. Roy, *Forced convection heat transfer in microencapsulated phase change material slurries: flow in circular ducts.* International Journal of Heat and Mass Transfer, 1991. **34**(3): p. 819.
11. Zhang, Y. and A. Faghri, *Analysis of Forced Convection Heat Transfer in Microencapsulated Phase Change Material Suspensions.* Journal of Thermophysics and Heat Transfer, 1995. **9**(4): p. 727.
12. Hao, Y.L. and Y.X. Tao, *A Numerical Model for Phase-Change Suspensions Flow in Microchannels.* Numerical Heat Transfer, Part A: Applications, 2004. **46**(1): p. 55.
13. Goel, M., S.K. Roy, and S. Sengupta, *Laminar forced convection heat transfer in microcapsulated phase change material suspensions.* International Journal of Heat and Mass Transfer, 1994. **37**(4): p. 593.
14. Roy, S.K. and B.L. Avanic, *Laminar forced convection heat transfer with phase change material emulsions.* International Communications in Heat and Mass Transfer, 1997. **24**(5): p. 653-662.
15. Inaba, H., M.-J. Kim, and A. Horibe, *Melting Heat Transfer Characteristics of Microencapsulated Phase Change Material Slurries With Plural Microcapsules Having Different Diameters.* Journal of Heat Transfer, 2004. **126**(4): p. 558-565.
16. Chen, B., et al., *An experimental study of convective heat transfer with microencapsulated phase change material suspension: Laminar flow in a circular tube under constant heat flux.* Experimental Thermal and Fluid Science, 2008. **32**(8): p. 1638.
17. Yamagishi, Y., et al., *Characteristics of microencapsulated PCM slurry as a heat-transfer fluid.* AIChE Journal, 1999. **45**(4): p. 696.
18. Wang, X., et al., *Flow and heat transfer behaviors of phase change material slurries in a horizontal circular tube.* International Journal of Heat and Mass Transfer, 2007. **50**(13-14): p. 2480.
19. Wang, X., et al., *Heat transfer of microencapsulated PCM slurry flow in a circular tube.* AIChE Journal, 2008. **54**(4): p. 1110-1120.
20. Hassanipour, F. and J.L. Lage, *New Bio-Inspired, Multiphase Forced Convection Cooling by ABS Plastic or Encapsulated Paraffin Beads.* Journal of Heat Transfer, 2010. **132**(7): p. 074501.
21. Ho, C.J., et al., *Water-based suspensions of Al2O3 nanoparticles and MEPCM particles on convection effectiveness in a circular tube.* International Journal of Thermal Sciences, 2011. **50**(5): p. 736-748.
22. Ho, C.J., et al., *On laminar convective cooling performance of hybrid water-based suspensions of Al2O3 nanoparticles and MEPCM particles in a circular tube.* International Journal of Heat and Mass Transfer, 2011. **54**(11–12): p. 2397-2407.
23. Ho, C., et al., *Forced convection performance of a MEPCM suspension through an iso-flux heated circular tube: an experimental study.* Heat and Mass Transfer, 2012. **48**(3): p. 487-496.
24. Takagi, J., et al., *Continuous particle separation in a microchannel having asymmetrically arranged multiple branches.* Lab on a Chip, 2005. **5**(7).
25. Di Carlo, D., et al., *Continuous inertial focusing, ordering, and separation of particles in microchannels.* Proceedings of the National Academy of Sciences of the United States of America, 2007. **104**(48): p. 18892.
26. Pamme, N. and A. Manz, *On-Chip Free-Flow Magnetophoresis: Continuous Flow Separation of Magnetic Particles and Agglomerates.* Analytical Chemistry, 2004. **76**(24): p. 7250.

DOI: 10.1016/j.ijheatmasstransfer.2012.09.014

Source: International Journal of Heat and Mass Transfer 56, no. 1–2, p. 380–389, 2013.

27. Petersson, F., et al., *Free Flow Acoustophoresis: Microfluidic-Based Mode of Particle and Cell Separation.* Analytical Chemistry, 2007. **79**(14): p. 5117.
28. Callen, H.B., *Thermodynamics and an introduction to thermostatistics*. 1985, New York: Wiley.
29. Maxwell, J.C., *A Treatise on Electricity and Magnetism*. 1881, Clarendon: Oxford.
30. Leal, L.G., *On the Effective Conductivity of a Dilute Suspension of Spherical Drops in the Limit of Low Particle Peclet Number.* Chemical Engineering Communications, 1973. **1**(1): p. 21.
31. Vand, V., *Theory of Viscosity of Concentrated Suspensions.* Nature, 1945. **155**(3934): p. 364.
32. Shah, R.K. and A.L. London, *Laminar Flow Forced Convections in Ducts*. Advances in Heat Transfer. 1978, New York: Academic Press. p.182.

DOI: 10.1016/j.ijheatmasstransfer.2012.09.014

Source: International Journal of Heat and Mass Transfer 56, no. 1–2, p. 380–389, 2013.

APPENDIX A

Model: Solution Methods, Assumptions and Validation

A.1 Momentum Equation

The simplified momentum equation (Eq. 5) is written separately for stream 1 (focused PCM suspension) and stream 2 (pure fluid):

$$\mu_1 \frac{\partial^2 u_1}{\partial y_1^{\,2}} = \frac{dP}{dx} \qquad 0 \le y_1 \le \delta \qquad \text{(A.1a)}$$

$$\mu_2 \frac{\partial^2 u_2}{\partial y_2^{\,2}} = \frac{dP}{dx} \qquad 0 \le y_2 \le H - \delta \qquad \text{(A.1b)}$$

where $y_2 = H - y_1$. These two equations are coupled through the following boundary conditions at the walls and at $y = \delta$:

$$\left.\frac{\partial u_1}{\partial y_1}\right|_{y_1=0} = 0 \qquad \text{(A.2a)}$$

$$\left.\frac{\partial u_2}{\partial y_2}\right|_{y_2=0} = 0 \qquad \text{(A.2b)}$$

$$\mu_1 \left.\frac{\partial u_1}{\partial y_1}\right|_{y_1=\delta} = -\mu_2 \left.\frac{\partial u_2}{\partial y_2}\right|_{y_2=H-\delta} \qquad \text{(A.2c)}$$

$$u_1|_{y_1=\delta} = u_2|_{y_2=H-\delta} \qquad \text{(A.2d)}$$

Eqs. 5 and A.1-2 are readily solved to obtain a fully-developed velocity profile depending on the viscosity ratio (μ_1/μ_2) and height ratio (δ/H), as shown in Figure A.1.

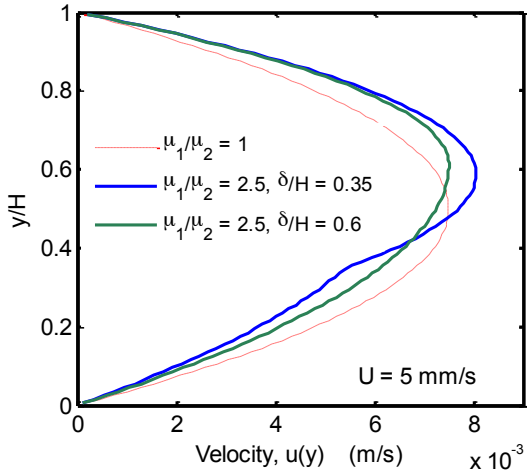

Figure A.1: Fully-developed velocity profile inside two-stream channel for the same mean fluid velocity (U = 5 mm/s) with different viscosity ratios (μ_1/μ_2) and height ratios (δ/H).

DOI: 10.1016/j.ijheatmasstransfer.2012.09.014

Source: International Journal of Heat and Mass Transfer 56, no. 1–2, p. 380–389, 2013.

A.2 Energy Equation

The overall energy equation for fully-developed laminar flow inside parallel plates with spatially-dependent and temperature-dependent thermophysical properties simplifies to Eq. 6. The fluid is assumed to enter the region of consideration at a uniform temperature (T_{in}).

$$T(0,y) = T_{in} \tag{A.3a}$$

The boundary conditions at the walls are incorporated as follows:

$$-k\left.\frac{\partial T}{\partial y}\right|_{y=0} = q'' \tag{A.3b}$$

$$\left.\frac{\partial T}{\partial y}\right|_{y=H} = 0 \tag{A.3c}$$

An analytical solution to Eqs. 6 and A.3 cannot be obtained due the temperature dependent heat capacity. Instead we solve the energy equations numerically. A finite difference scheme is used to solve the equations and the boundary conditions along the *y*-direction with thermophysical properties defined at each node according to the nodal spatial location and temperature, while the 4th order Runge-Kutta method is used to step explicitly along the x-direction. A mesh refinement study along the *y*-direction was performed until the maximum variance in the *Nusselt* number is below 0.01%. The model is validated against an analytical solution for the developing local *Nusselt* number below such that it can confidently be used to simulate the effect of phase-change particles on the local heat transfer coefficient.

A.3 Brownian Diffusion of PCMs

Neglecting diffusion of PCMs across the two streams over the characteristic length of PCM melting is justified as described below:

The amount of time needed to fully melt the PCM particles (t_{melt}) can be approximated from an energy balance by dividing the energy required to melt the particles by the heat supplied from the bottom wall. For asymmetrically heated parallel plate geometries, this expression simplifies to the following:

$$t_{melt} \approx \frac{\rho_f H \omega h_{sf}}{q''} \tag{A.4}$$

The diffusion length (δ_B) of PCM microparticles through Brownian (random) motion during the melting time can be expressed as:

$$\delta_B \approx \sqrt{D_B t_{melt}} \tag{A.5}$$

where the Brownian diffusion coefficient, D_B, is given by the Einstein-Stokes equation:

DOI: 10.1016/j.ijheatmasstransfer.2012.09.014

Source: International Journal of Heat and Mass Transfer 56, no. 1–2, p. 380–389, 2013.

$$D_B = \frac{k_B T}{3\pi\mu_f d_p} \tag{A.6}$$

and k_B is the Boltzmann constant, μ_f is the basefluid dynamic viscosity, and d_p is the diameter of a PCM microparticle. If we compare the PCM diffusion length (δ_B) to the channel height, H, we obtain the following ratio:

$$\frac{\delta_B}{H} \approx \sqrt{\frac{k_B T \rho_f \omega h_{sf}}{3\pi\mu_f d_p q'' H}} \tag{A.7}$$

For typical values used in the manuscript (*i.e.*, ρ_f = 992 kg/m^3, μ_f= 6.36·10^{-4} Pa·s, h_{sf} = 150 kJ/kg, ω= 0.10, q''= 5 kW/m^2, H = 0.5 mm) at a temperature of 313 K and with 1 μm particles, δ_B/H is approximately 0.002. In other words, the typical PCM interdiffusion length considered in the study is approximately 1 μm, which is negligible compared to the channel height (0.5 mm). Thus, diffusion between the two streams (*i.e.,* PCM diffusion) can be neglected.

A.4 Validation

To validate the numerical model, we compare it to a known analytical solution on the basis of local *Nusselt* number (Eq. 7). Figure A.2 shows Nu_x obtained using the numerical model for a thermally-developing flow between parallel plates with constant heat flux from both walls. The result is compared to a correlation recommended by Shah and London which is based on the infinite series analytical solution. The numerical model follows the analytical correlation exactly, thus, validating the accuracy of the numerical model and its ability to model thermally-developing flows.

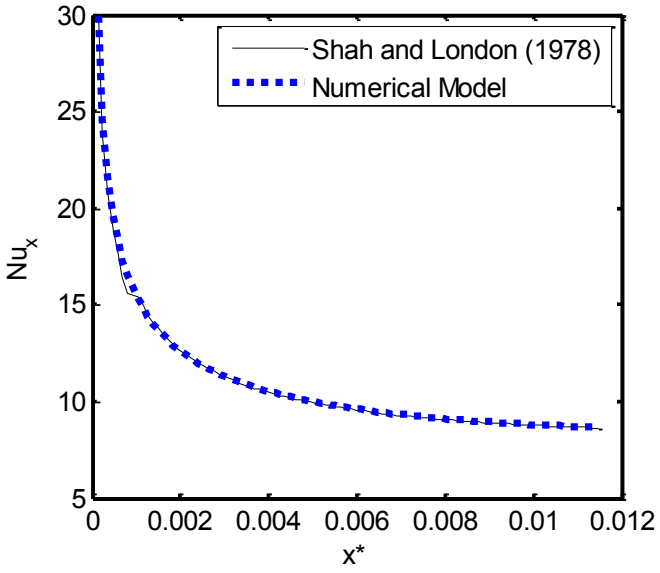

Figure A.2: Thermally-developing local *Nusselt* number (Nu_x) as a function of the dimensionless length (x^*); comparing the numerical model (this study) with the analytical solution [32].

DOI: 10.1016/j.ijheatmasstransfer.2012.09.014

Source: International Journal of Heat and Mass Transfer 56, no. 1–2, p. 380–389, 2013.

APPENDIX B

Prediction Results

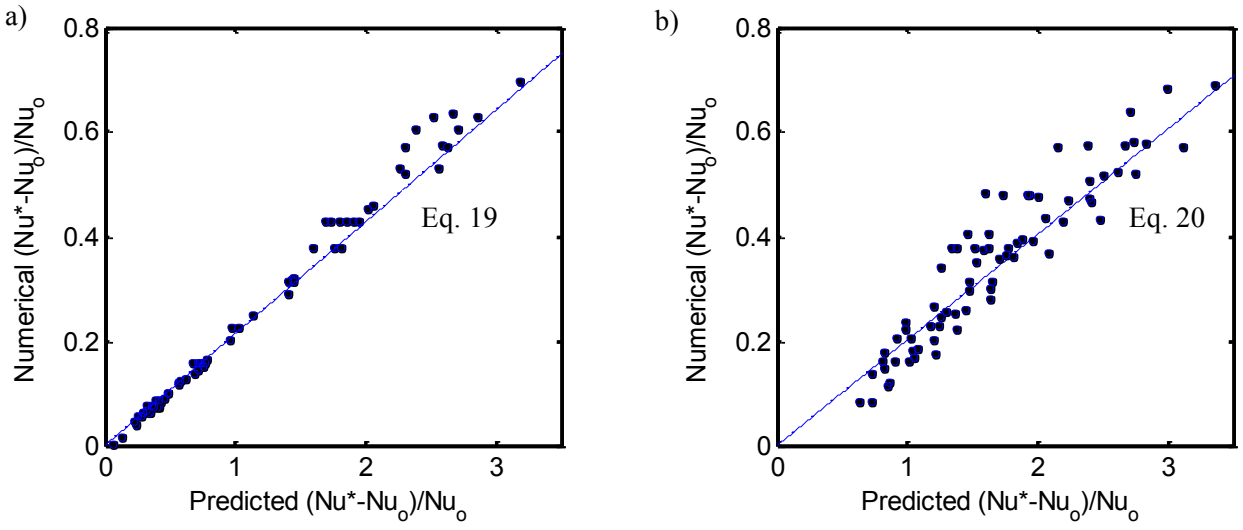

Figure B.1: Simulation results for *Nu enhancement compared to the predicted values based on: a) Eq. 19 (*Mr* < 1), b) Eq. 20 (*Mr* > 1).**

Eqs. 19 - 20 were obtained by determining a line of best fit between the simulation results and a power law expression involving the appropriate dimensionless quantities. For the low *Mr* case (Figure B.1a), the prediction (Eq. 19) matches well with the results as quantified by the high R^2 value (0.99). In the high *Mr* range (Figure B.1b), the proposed expression (Eq. 20) generally agrees with the numerical results; however, a higher uncertainty is observed (R^2 = 0.86) which is most likely because the shape of the effective heat capacity has a complex effect on the magnitude of the *Nu** enhancement in this regime.